

We are IntechOpen, the world's leading publisher of Open Access books Built by scientists, for scientists

6,900

Open access books available

185,000

International authors and editors

200M

Downloads

Our authors are among the

154

Countries delivered to

TOP 1%

most cited scientists

12.2%

Contributors from top 500 universities



WEB OF SCIENCE™

Selection of our books indexed in the Book Citation Index
in Web of Science™ Core Collection (BKCI)

Interested in publishing with us?
Contact book.department@intechopen.com

Numbers displayed above are based on latest data collected.
For more information visit www.intechopen.com



Applications of Dielectric Barrier Discharge Microplasma

Kazuo Shimizu, Jaroslav Kristof and Marius Gabriel Blajan

Abstract

Dielectric barrier discharge microplasma is a nonthermal plasma discharge at atmospheric pressure which due to the micrometer size dielectric layer between the grounded and high-voltage energized electrodes enables to drive the device at less than 1 kV. Microplasma is an economical and ecological alternative for conventional technologies used for NO_x removal, indoor air cleaning, surface treatment of polymers, biomedical applications such as transdermal drug delivery, or as an actuator. In this chapter, microplasma applications such as indoor air purification, skin treatment for drug delivery, particle removal, and flow control are presented.

Keywords: dielectric barrier discharge, microplasma, indoor air purification, plasma drug delivery, particle removal, electrohydrodynamic flow, plasma actuator

1. Introduction

Microplasma is a term used typically for referring to gas discharges that have dimensions ranging from few micrometers up to few millimeters. The breakdown voltage which is the voltage that is required to ignite a discharge depends on the product of pressure p and discharge gap d , that is also known as the Paschen curve. According to the Paschen curve, at atmospheric pressure, the breakdown voltage can be kept at low values if the discharge gap is below 1 mm. Thus the typical operating parameters of microplasmas (pressures up to and exceeding 1 atmosphere and discharge gaps below 1 mm) correspond to the values of p and d product similar to the values of the large-volume low-pressure plasmas but with much higher energy densities [1–3]. The microplasma presented in this chapter is a nonthermal plasma discharge at atmospheric pressure. It is a type of dielectric barrier discharge (DBD) generated using a configuration having a dielectric material covering the electrodes and a narrow discharge gap of micrometer size between electrodes. Because it is generated at relatively low discharge voltages of about 1 kV, the reactor has small dimensions and requires only small-sized power supplies. Considering the electrodes covered by a dielectric layer with a dielectric constant of $\epsilon_r = 10^4$ and according to the law that states the electric displacement field inside the capacitor formed by the two dielectric layers and the air gap is constant, it results in the air gap an electric field 10^4 times higher than the electric field in the dielectric layers. At a discharge gap of 10 μm , it has obtained a high electric field $E = 10^7\text{--}10^8$ V/m that assures the formation of nonthermal plasma at a discharge voltage about 1 kV. The temperature estimation of the microplasma discharge using emission spectroscopy shows high electron and low rotational temperatures. These temperatures are specific for nonequilibrium plasmas [4].

Despite the small size, the development still continues in order to improve the technology and further miniaturization.

As a technology for indoor air purification [5–7], microplasma was used to remove hexadecane ($C_{16}H_{34}$) which is a semivolatile organic compound (SVOC) that has its origin from diesel oil [8–11]. Due to the exhaust gases present in the atmosphere, the hexadecane also enters indoors. The concentration of hexadecane decreased from 3000 to 105 ppm after 120 minutes of microplasma processing.

In the field of transdermal drug delivery and cosmetics, microplasma can change the surface properties of the skin and increase adsorption of relevant substances that are important for creams, detergents, and other formulations applied on the skin surface [12–15]. Moreover, changes in the lipid barrier of the skin induced by microplasma can make it easier to incorporate molecules in the skin or through the skin.

Microplasma can be used as a technology for particle removal. The removal or transfer of fine particles is important for global environmental problems such as PM 2.5, semiconductor industry dust contamination, [16] or for the exploration activities on the moon [17, 18]. Due to the electrostatic and dielectrophoretic forces, particles can be removed from surfaces of solar cells or from components in electronic industry in the case of dust contamination [19–21].

Microplasma actuator is a technology that can replace mechanical actuators. Due to the lack of moving parts and fast response, it has advantages over the conventional actuators [22–24]. The electrohydrodynamic (EHD) phenomenon, which occurs due to the momentum transfer from ions accelerated by an electric field to neutral molecules by collision, generates flow. A multielectrode geometry of the microplasma actuator and the possibility to drive various parts of the actuator independently using FET switches were used; thus the flow direction was controlled. The flow characteristics at various time intervals were measured by a high-speed camera. The small dimension of microplasma actuator and the light emission near the active electrodes make the experimental investigation near the electrodes difficult. Numerical simulation software based on the Suzen-Huang model coupled with Navier-Stokes equations was developed; thus additional information about the flow characteristics was obtained near the electrodes due to numerical simulation [25–27].

With these applications, microplasma technology has proven to be a reliable alternative for a wide range of conventional technologies with advantages of being ecological, economical, and easy to integrate with other systems.

2. Applications of dielectric barrier discharge microplasma

Various applications of dielectric barrier discharge microplasma make this technology a versatile and effective tool used for indoor air purification, transdermal drug delivery, particle removal, or flow control.

2.1 Indoor air purification

Indoor air quality (IAQ) is an important factor for a healthy life because people spend a major part of their time inside buildings. Among the factors that worsen the IAQ are smells, fine particles, and various chemical substances [5–7]. Technologies for purifying the indoor air are studied, and equipment is already on the market. Plasma is a technology that is applied for air purification. The main nonthermal technologies for air purification could be roughly classified in methods using dielectric barrier discharge [28, 29] and corona discharge [30, 31]. Each method has advantages, but the dielectric barrier discharge is more suitable to an easy

integration in other systems. Moreover dielectric barrier discharge microplasma has a discharge gap of micrometer order and requires a discharge voltage of about 1 kV; thus only a small-sized power supply is needed. Various active species, ozone (O₃), and ultraviolet light (UV) are generated by plasma discharge in air at atmospheric pressure [8, 9]; thus chemical substances can be decomposed or bacteria sterilized [10, 11]. One of the substances that are studied to be decomposed by microplasma is hexadecane (C₁₆H₃₄) [32–34]. Hexadecane is a semivolatile organic compound (SVOC), and because it is present in diesel oil, it enters inside buildings from outside. A bad smell is caused by hexadecane and also affects the respiratory organs. It is a large-molecular-weight substance and thus not easy to decompose because of many carbon–carbon bonds that are strong and have low chemical reaction.

The results of the hexadecane removal process by microplasma were investigated by using the Fourier transform infrared spectroscopy (FTIR) (SHIMADZU, Kyoto, Japan, FTIR-8400S), and a gas chromatograph-mass spectrometer (GC-MS) (SHIMADZU, GCMS-QP2010). For the GC-MS measurements, nonpolar columns (Restek, Bellefonte, PA, USA, Rxi-1ms fused silica capillary column (30 m × 0.25 mm ID, 0.25 µm film thickness)) consisting of Crossbond (dimethyl polysiloxane) were used.

2.1.1 Microplasma electrode for indoor air purification

The microplasma electrode used for the hexadecane removal process is shown in **Figure 1**. Two metallic electrodes with 1 mm thickness, perforated with holes ($\phi = 5$ mm, aperture ratio: 41.5%), are coated with dielectric. A 30-µm gap is obtained in between the electrodes and using a resin at periphery to fix them. Plasma was generated around the holes and in between the electrodes while the gas flowed through the holes and was processed by microplasma discharge [35–37]. The microplasma discharge started when applying a sinusoidal voltage with amplitude 400 V₀ – p (0 to peak) and frequency 27 kHz in air using a neon transformer.

Applied voltage was controlled using a variable autotransformer.

The waveforms of voltage and corresponding current when the electrode was energized at 550 V₀ – p in air are shown in **Figure 2**. The spikes convoluted in the current waveform appeared due to plasma generation.

2.1.2 Hexadecane decomposition

The following process was used for hexadecane removal using the microplasma electrode:

1. The microplasma electrode was placed inside the small chamber (11.4 L), and the chamber was closed.
2. About 3000 ppm of hexadecane was vaporized in the chamber.
3. The voltage applied to the microplasma electrodes for 120 minutes was 550 V₀ – p.

Pure air (CO < 1 ppm, CO₂ < 1 ppm, THC < 1 ppm) from the gas cylinder was used. The amount of hexadecane before and after microplasma treatment was measured by using FTIR. The spectrum before and after vaporizing 3000 ppm of hexadecane in the chamber filled with room air (40–50%RH) is shown in **Figure 3**. In the upper part of the figure, using arrows, the alkanes or alkenes which were generated during the vaporization process of hexadecane are shown.

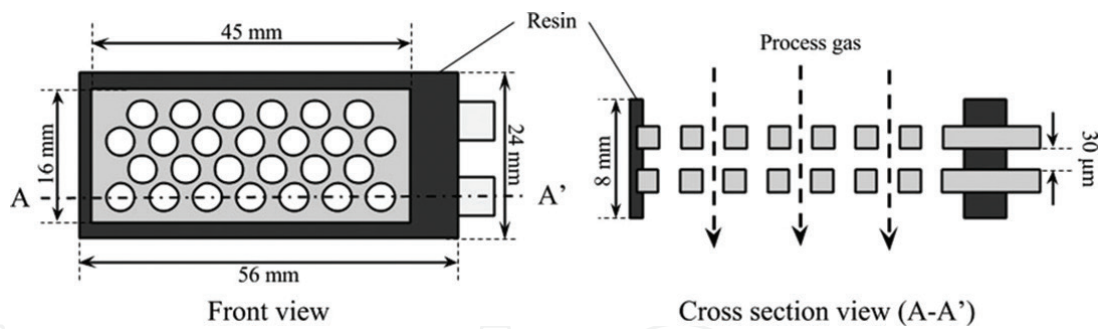


Figure 1. Microplasma electrode.

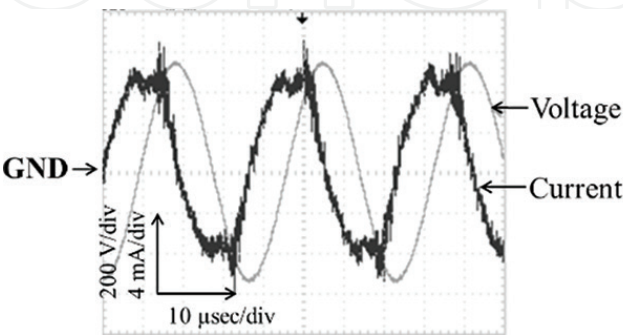


Figure 2. Waveforms of discharge voltage and corresponding discharge current.

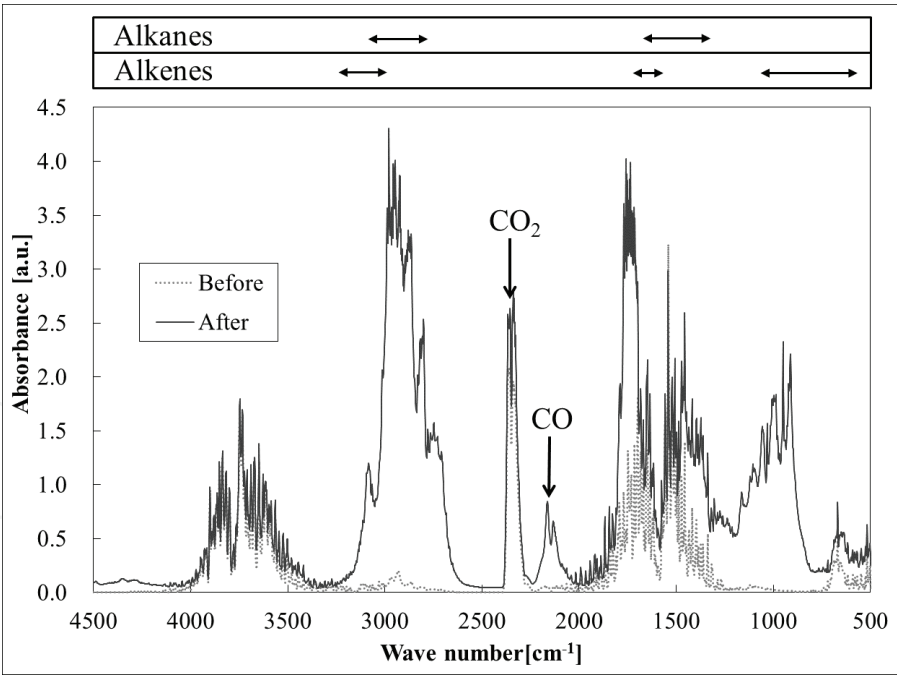


Figure 3. Spectrum before and after vaporizing of hexadecane.

In **Figure 4**, the FTIR spectrum obtained before and after 120 minutes without using microplasma in the chamber filled with room air and containing 3000 ppm of hexadecane is shown. The spectrum after 120 minutes is the “natural decay.” Even without the microplasma, hexadecane decreased after vaporization due to the condensation on the chamber walls. In **Figure 5**, the spectrum before and after 120 minutes of plasma processing in the chamber filled with room air and an initial concentration of 3000 ppm of hexadecane is shown.

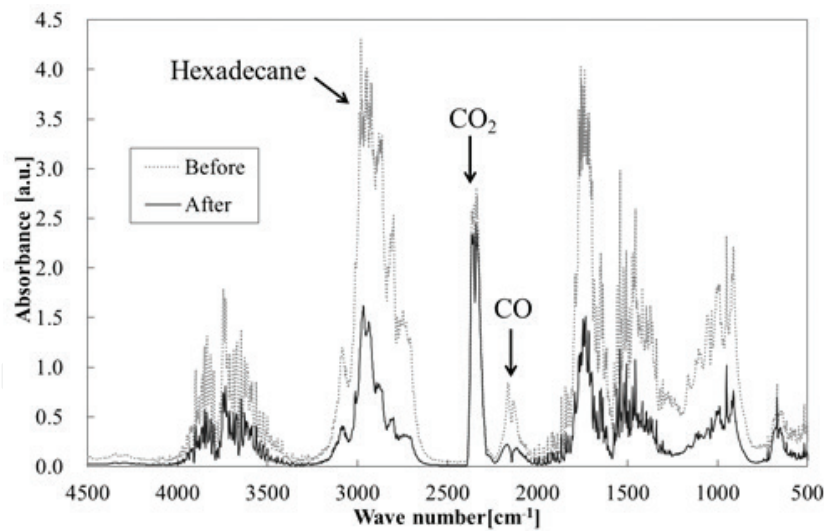


Figure 4.
Spectrum before and after 120 minutes without the plasma processing.

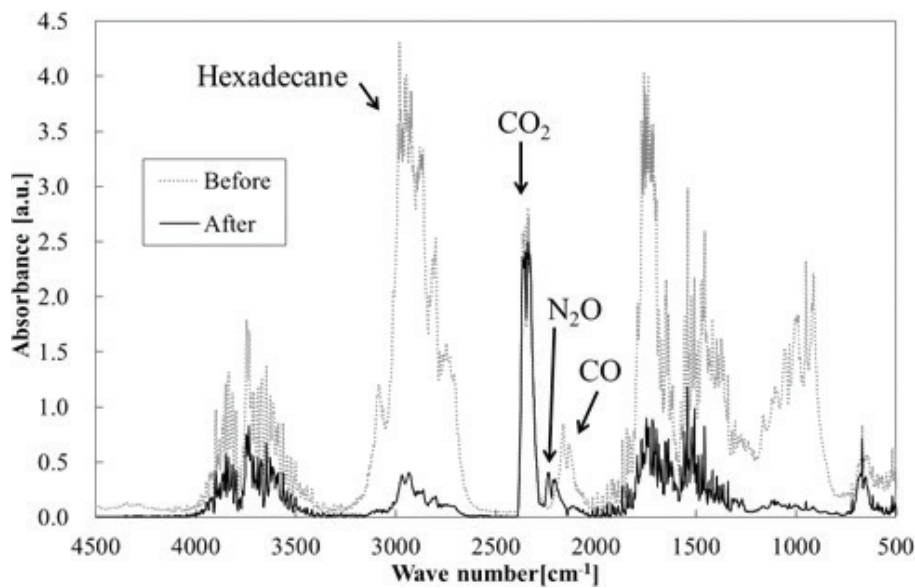
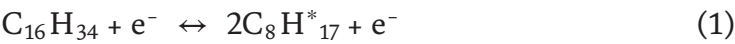


Figure 5.
Spectrum before and after 120 minutes of plasma processing.

The peak of vibrational band corresponding to hexadecane and CO decreased after microplasma treatment and that of N₂O increased. The FTIR measurement of other bands was difficult due to overlapped spectra. The hexadecane concentration was carried out by using the maximum peak in the 2984–2833 cm⁻¹ range. The variation of hexadecane concentration with the microplasma process time is shown in **Figure 6**. The values are lower than in the case of natural decay. From an initial concentration of 3000 ppm, the hexadecane decreased to 150 ppm after the microplasma process for 120 minutes. By comparison the natural decay was to 950 ppm after 120 minutes; thus microplasma decomposed the hexadecane. The removal energy efficiency of hexadecane was calculated at 19.8 µg/W h. Eqs. (1)–(3) explain the hexadecane decomposition process. Microplasma is a nonequilibrium plasma under atmospheric pressure; thus active species and high-energy electrons generated by microplasma decompose the hexadecane [38]. At the interaction with an electron, the hexadecane breaks in two neutral radical molecules:



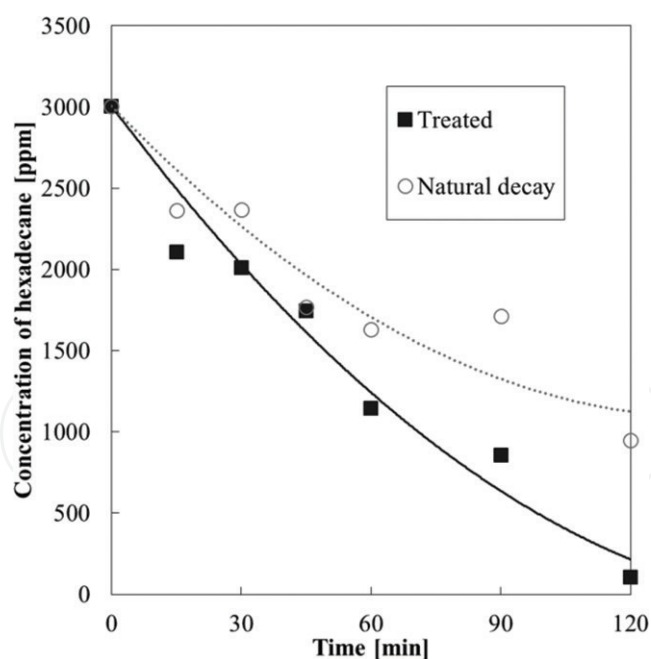


Figure 6.
Concentration of hexadecane with processing time.

Anionic or cationic carbon species could be also obtained after electron impact:



The loss of a proton generates alkene:



Due to the active species generated by microplasma, the carbon single bonds were cut, and substances that have less carbon atoms were formed as intermediate products. To conclude, after the microplasma process of hexadecane removal, the following results were obtained:

1. The hexadecane concentration was decreased from the initial value of 3000 ppm to 150 ppm after the 120 minutes of microplasma treatment. In comparison, the natural decay was to 950 ppm; thus microplasma decomposed the hexadecane.
2. The removal energy efficiency of hexadecane was calculated at 19.8 $\mu\text{g}/\text{W h}$.

2.2 Skin treatment by plasma for drug delivery

A new method of drug delivery through the skin is plasma by modifying the skin permeability [12–15, 39–41]. Researchers were investigating the phenomena of interaction between the plasma and the skin. The penetration of the reactive oxygen species (ROS) using plasma jet with discharge gas helium was investigated by Szili et al. [42]. Another study where bovine keratin taken as a model protein was subject to dielectric barrier discharge plasma treatment and showed the generation of cysteic acid by oxidation of disulfide bonds accompanied by a decrease in pH [43]. The human forearm was treated by dielectric barrier discharge plasma and an increased number of C—O and C=O bonds, and a decreased number of C—C

bonds in the lipids were measured after the treatment as reported by Marschewski et al. [44]. Various processes were used for the enhancement of skin permeability such as chemical solutions, ablation, iontophoresis, or electroporation [45].

The influence of argon plasma on the thickness on the stratum corneum layer and extraction of lipids from stratum corneum was investigated. Attenuated total reflectance-Fourier transform infrared (ATR-FTIR) spectroscopy and section measurement of skin were used for measuring the modifications caused by plasma in the stratum corneum layer. Only lipophilic molecules and molecules with weight less than 500 g/mol can penetrate through the skin because of the stratum corneum, a lipid-rich matrix with embedded corneocyte cells. The majority of active agents for therapeutic applications are represented by relatively large drugs; thus the low permeability is problematic. Skin permeability was studied using attenuated total reflectance-Fourier transform infrared spectrometry. Information about the chemical structure of lipids and their amount in the stratum corneum could be obtained by studying the spectra of the skin. Also, the microscopic observation could give information about the morphologic changes across a section of the skin. The etching of the skin, lipid extraction, and appearance of the skin after atmospheric pressure argon plasma treatment were investigated.

2.2.1 Experimental setup

The schematic image of the experimental setup using the plasma jet is shown in **Figure 7(a)**. Nonthermal plasma was generated at atmospheric pressure by a plasma jet type structure consisting of a Pyrex tube (outer diameter 6 mm, length 100 mm) and a central tungsten (0.8 mm in diameter) high-voltage (HV) electrode covered by a glass layer except for a 10-mm long region close to outlet of Pyrex tube. The grounded electrode was an aluminum ring (8 mm diameter) located on the outer surface of the Pyrex tube at 12 mm from the end of the plasma jet. The electrodes were energized using a Neon transformer (ALPHA Neon M-5) with an AC voltage with frequency of 16 kHz. The voltage and current were measured using a Tektronix P60015A high-voltage probe and a Tektronix P6021 current probe. A grounded

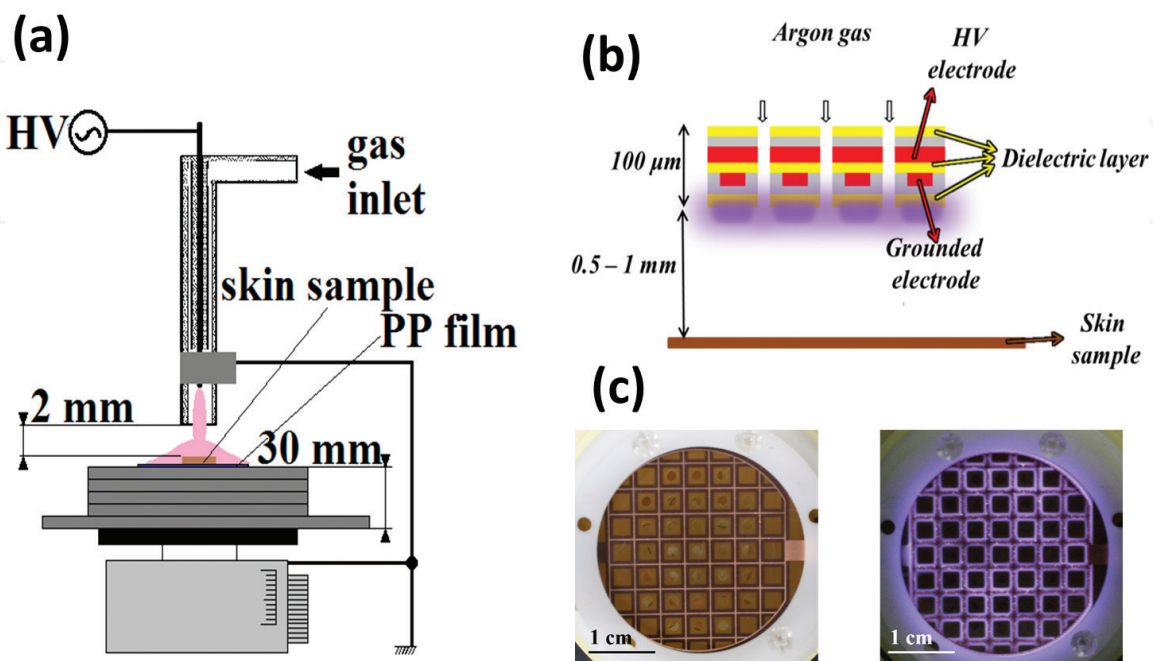


Figure 7. Experimental setup for plasma treatment of skin: (a) plasma jet; (b) microplasma and (c) photo of microplasma electrode without and with discharge.

micrometric sample holder was used to set the distance between the skin sample and the outlet of the plasma jet at 2 mm, and a 30-mm thick PVC insulator was used to insulate the sample from the holder.

The plasma treatment was carried out for 1 minute, and the sample was in contact with plasma during this time. Argon gas (purity 99.99%) was flowed through a Yamato flow meter in to the plasma jet. The upper layer of stratum corneum of pig skin was observed by attenuated total reflectance-Fourier transform infrared (ATR-FTIR) spectrometer (Jasco FT/IR 6300 with ATR PRO610P-S) with a diamond prism, and the spectra were recorded with a resolution of 8 cm^{-1} and by accumulating 150 scans.

Yucatan micropig skin from Charles River Laboratories Japan, Inc. (Yokohama, Japan) was used for experiments of the plasma treatment. The skin was stored at -20°C in a freezer before the experiments. The pig skin preparation procedure was first, the fat layer of the skin was removed by using a knife, then it was cut and soaked at 4°C in phosphate buffered saline (PBS) for 3 hours, and then after a bath in 60°C PBS for 1 minute, the epidermal layer of a thickness of $200\text{ }\mu\text{m}$ was peeled using tweezers. Finally the skin sample was cut in to $3 \times 3\text{ mm}$ parts and attached to a polypropylene film by using double-sided tape.

A dielectric barrier discharge microplasma was generated by a thin-film electrode with a thickness of $105\text{ }\mu\text{m}$ is shown in **Figure 7(b)** and **(c)**. Both high-voltage and grounded electrodes were encapsulated in the dielectric. The thickness of electrodes was $18\text{ }\mu\text{m}$ separated by a $14\text{ }\mu\text{m}$ thick dielectric. The outer side of each electrode was covered by a dielectric with a thickness of $27.5\text{ }\mu\text{m}$. Plasma was generated at the surface closer to the grounded electrode. Atmospheric argon plasma was generated at a voltage of 950 V and a frequency of 25 kHz using a Neon transformer (ALPHA Neon M-5, LECIP). Gas flow of argon was set to 5 l/minute using a flow meter (Yamato). The treatment time of the skin was set to 5 minutes after the gas flow was started. The thickness of the plasma was negligible in comparison with the distance between the electrode and the skin surface, which was set to 0.5–1 mm. Thus, the plasma was not in contact with the skin.

2.2.2 Skin treatment by plasma for transdermal drug delivery

A microscope was used to visualize a microscale change in the stratum corneum; thus the paraffin-embedded skin samples were sectioned at a thickness of several micrometre using a microtome and were placed on a glass slide.

Figure 8a shows the untreated sample, and **Figure 8b–d** shows the images of sample treated for 10 s, 30 s, and 60 s at a voltage of 4 kV amplitude. A disruption of the stratum corneum layer on the treated samples is observed. The upper layer of stratum corneum was detached and the thickness decreased.

The ATR-FTIR spectra of the pig skin stratum corneum samples before and after the plasma jet treatment were compared.

The asymmetric stretching band of CH_2 ($2917\text{--}2923\text{ cm}^{-1}$) was examined due to a highest absorbance of the band. The electrodes were energized at 4 kV amplitude, and the skin samples were measured at various treatment times from 10 s to 15 minutes.

The extraction of lipids with treatment time and saturation of their extraction after 120 s are shown in **Figure 9**.

The thickness of the stratum corneum decreased to $11\text{ }\mu\text{m}$ after 60 s of plasma treatment. The skin barrier effect depends on the thickness of the stratum corneum and the amount of lipids and their structure; thus the barrier function of the skin was reduced. The etching effect could be attributed to the ions or radicals created in the plasma.

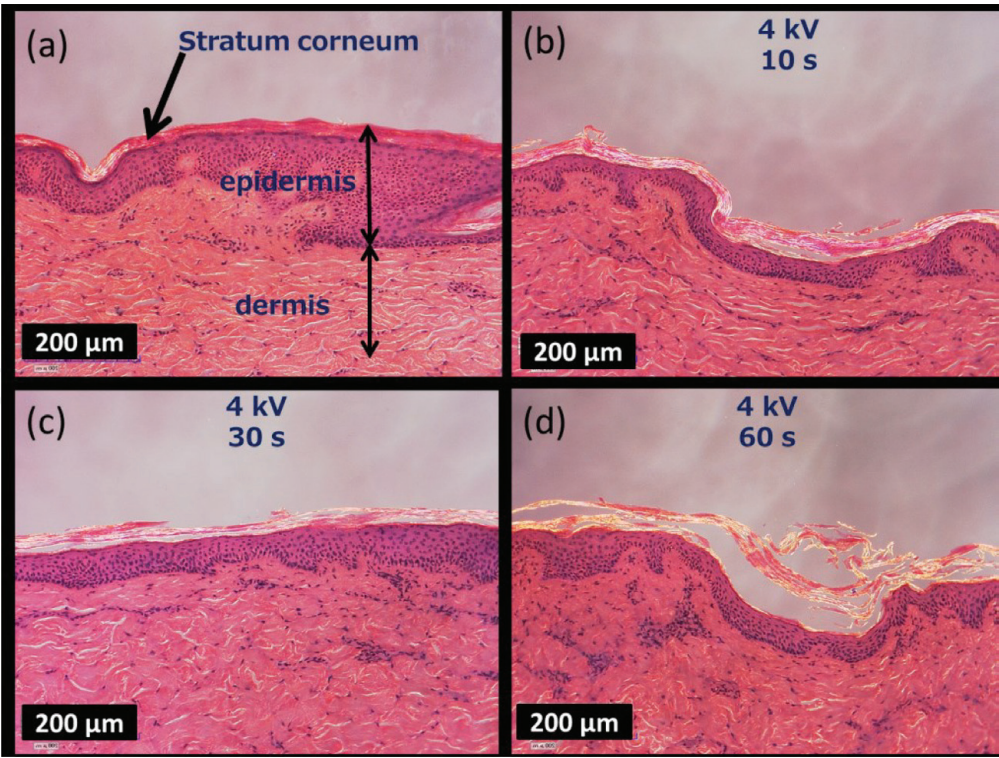


Figure 8. Section of skin samples. (a) Untreated sample, (b) dielectric barrier discharge argon plasma treatment for 10 s at 4 kV, (c) dielectric barrier discharge argon plasma treatment for 30 s at 4 kV, and (d) dielectric barrier discharge argon plasma treatment for 60 s at 4 kV.

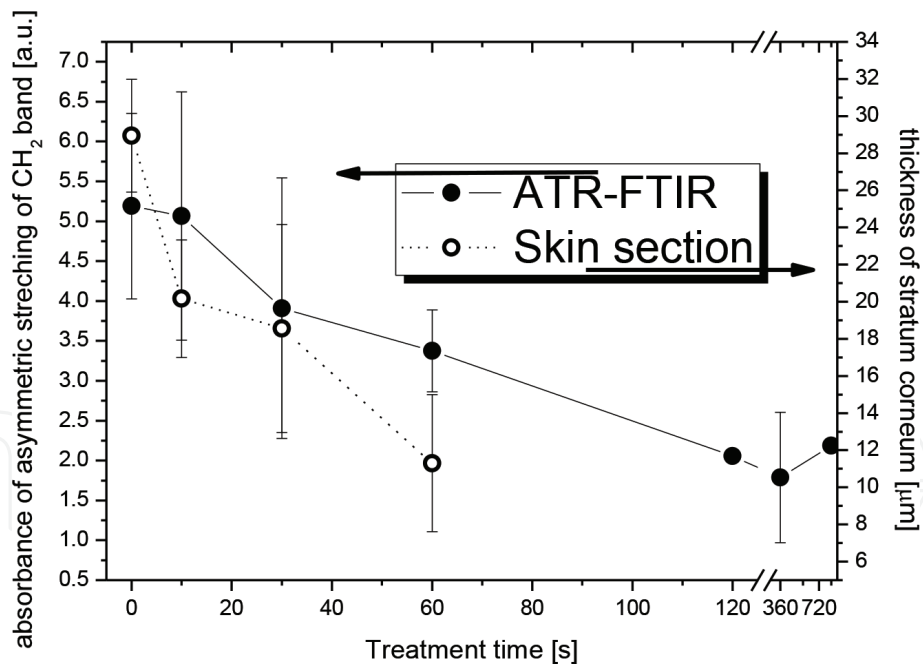


Figure 9. Evolution of absorbance of the asymmetric stretching band of CH₂ after various times of treatment (black circles). Evolution of thickness of stratum corneum (empty circles).

Because of skin regeneration, the upper cells of the skin are attached weaker than the deeper layers; thus the etching effect can be nonlinear. The extraction of lipids and its saturation are different for the layers which are not in contact with plasma. A relatively long-term effect of plasma was measured, and the description of a fast effect of plasma treatment that can increase permeability of the skin was not carried out.

After the experiments of atmospheric pressure plasma jet treatment of pig skin, the disruption of stratum corneum was measured. It was found that after 30 s of treatment, the skin was disrupted, and ATR-FTIR measurements confirmed the extraction and also the saturation of etching after 120 s. The thickness of the stratum corneum was decreased to one third ($11\text{ }\mu\text{m}$) of the original thickness after 60 s of treatment.

The treatment of the skin by dielectric barrier discharge microplasma was carried out. Full-thickness (dermal + epidermal layer) skin was cut to ultrathin sheets by ultramicrotome to observe the lamellar structure of the lipid matrix. This matrix can be observed as bright lines with dark space in between. Bright lines represent lipid tails and dark spaces represent hydrophilic heads [46]. Unaltered lipid lamellae are shown in **Figure 10**.

Lipid lamellae of microplasma-treated skin shows disturbed areas (nonhomogeneous) of lipid membrane with lacunar space along corneocytes and also extracted

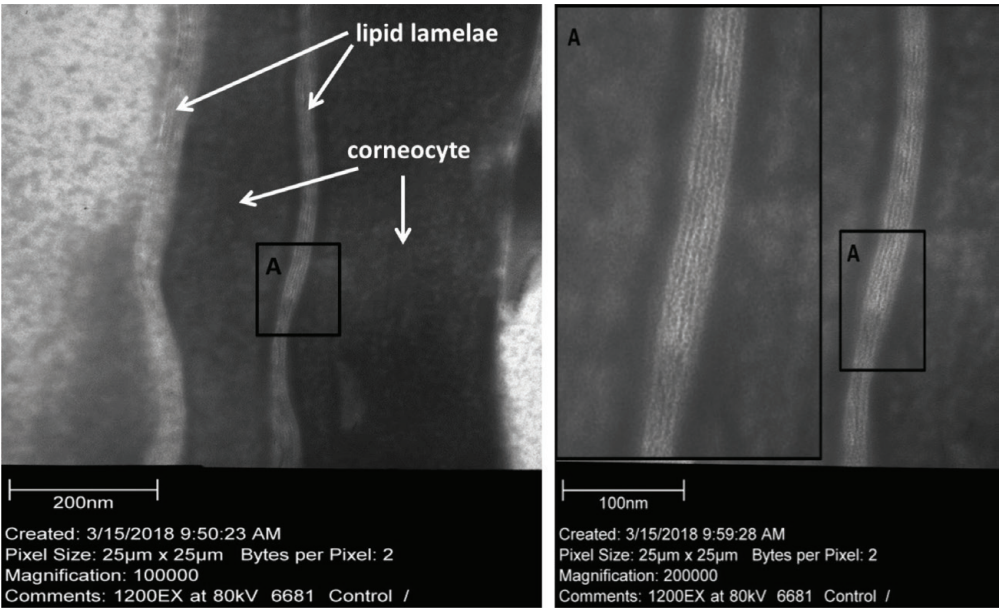


Figure 10.
Lipid lamellae of untreated skin sample with detail in A.

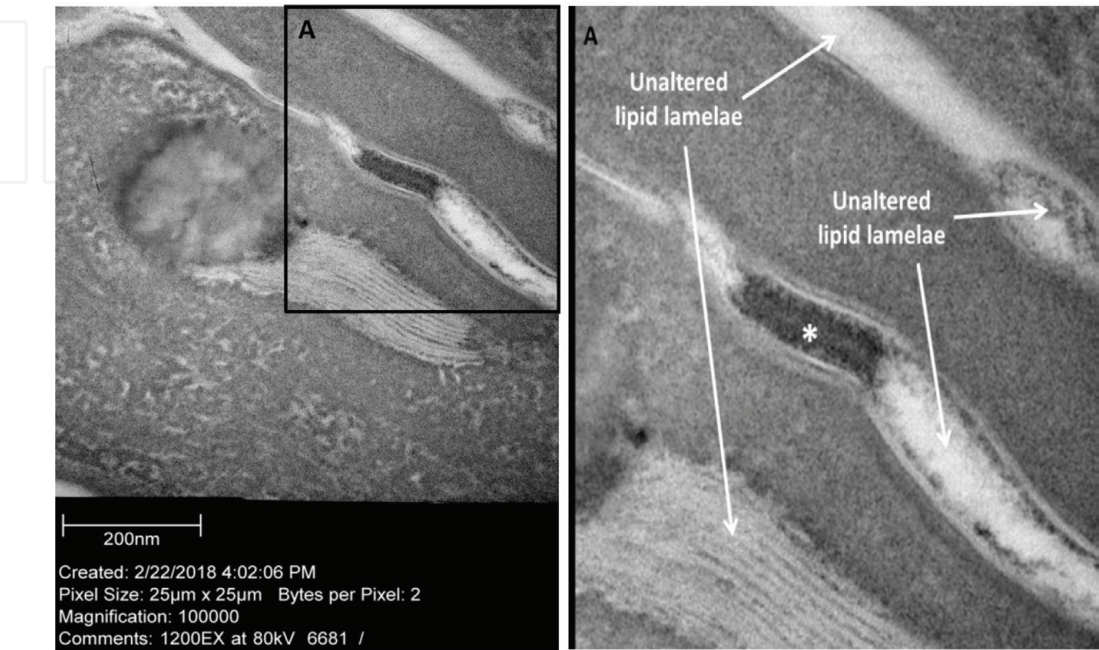


Figure 11.
Lipid lamellae of microplasma-treated skin sample with detail in A. Asterix—space without lipid lamellae.

lipids in “asterix” space in **Figure 11**. The skin was treated for 5 minutes by argon microplasma.

The results obtained using plasma jet and microplasma showed the modification of the skin in order to carry out the transdermal drug delivery.

2.3 Particle removal

Plasma technology was applied for the removal or collection of fine particles. Microplasma electrode was used to remove the fine particles from the electrode surface due to the action of electrostatic forces. Microplasma [47] was already proved to be an economical and ecological solution in the case of biomedical applications [1, 48], surface treatment [49], material synthesis [50], and indoor air treatment [33]. The removal or transfer of fine particles is important for global environmental problems such as PM 2.5, semiconductor industry dust contamination [16], or for the exploration activities on the moon [17, 18]. Research results regarding the dust removal process using dielectrophoretic and electrostatic forces were published by Calle et al. [18] and Kawamoto et al. [19]. Because the charged or uncharged lunar dust has a negative influence on the operation of mechanical system, lunar dust simulant was used in the series of experiments. Also, other researchers investigated removal of the fine particles from the surface of solar cells [20, 21], the transport of toner particles by traveling wave [51, 52] and the decontamination of the silicon wafer [53, 54]. Due to its advantages such as low discharge voltage of about 1 kV and scalability of electrode size, microplasma was used for particle removal [55]. An AC voltage with amplitude 1 kV was applied to microplasma electrodes in order to remove SiO₂ particles from their surface. The dependency of the particle removal with the frequency of applied voltage was investigated.

2.3.1 Microplasma electrode for particle removal

For particle removal experiments, the microplasma electrode shown in **Figure 12** was used [55].

The electrode structure consists of strip-type electrodes (top-side electrode), a plate-type electrode (bottom-side electrode), a dielectric layer, and an isolating layer.

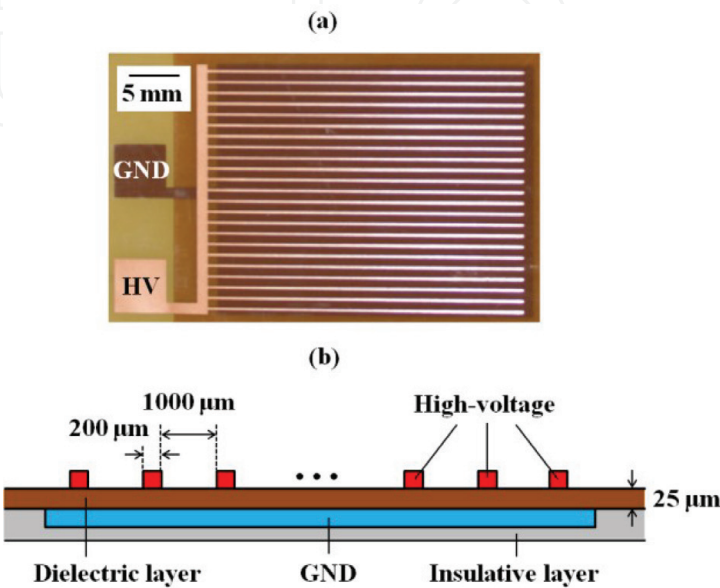


Figure 12.
Schematic images of the microplasma electrode: (a) top view and (b) cross section view.

For the stripe-type electrodes, copper was used and as a dielectric layer polyimide. The microplasma electrode has a capacitive load of 200 pF. The top-side electrode consisted of 23 stripes with 1 mm in between and was energized at high-voltage (HV), and the plate type bottom-side electrode was grounded. The top strip-type electrodes' width and length were 200 μm and 30 mm, respectively. The plate-type electrode area was $23 \times 30 \text{ mm}^2$. The dielectric in between the HV electrode and grounded electrode had 25 μm thickness; thus plasma could be generated at a discharge voltage of about 1 kV. The experimental setup for the fine particle movement experiments is shown in **Figure 13**. The HV electrode was energized by an AC voltage with 1 kV amplitude, and the frequency was varied from 10 Hz to 10 kHz. The voltage was obtained using a function generator (Tektronix AFG3102) and a HV power amplifier (TREK 5/80).

A high-voltage probe (Iwatsu HV-P30) and an oscilloscope (Tektronix TDS 2014) were used for the measurement of applied voltage. For the measurements of the discharge current, a resistor was connected between the electrode and ground. The voltage drop on the resistor was measured using a voltage probe (Tektronix P2220) and an oscilloscope (Tektronix TDS 2014), and thus the current was obtained by Ohm's law. The particles used in the series of experiments were SiO_2 particles (diameter, 50 μm ; density, 2.2 $\text{g} = \text{cm}^3$; and shape, spherical).

For each experiment, 60 mg of SiO_2 particles were placed on the electrode surface before applying the AC voltage (applied to the electrodes for 3 minutes). The waveforms of applied voltage and discharge current are shown in **Figure 14** for the frequency of the applied voltage 50 Hz, 500 Hz, and 5 kHz.

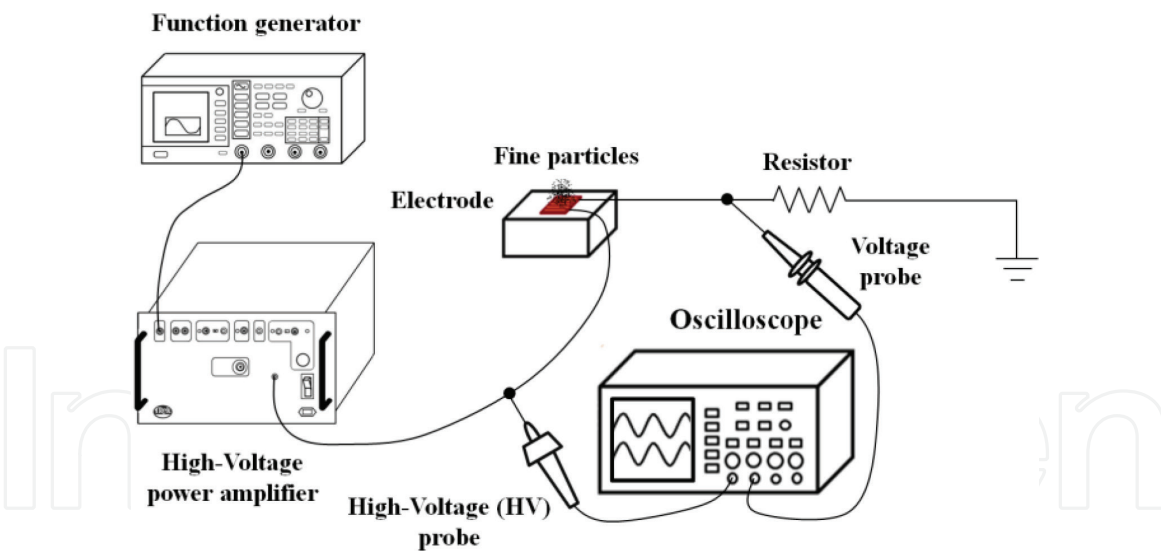


Figure 13.
Experimental setup for observing fine particle movement.

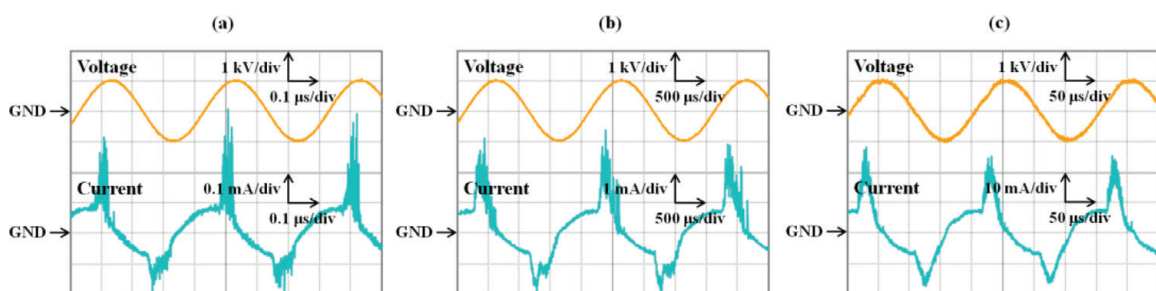


Figure 14.
Waveforms of the applied voltage and the discharge current at (a) 50 Hz, (b) 500 Hz, and (c) 5 kHz.

The discharge current had two components: the capacitive current (due to the capacitance of the electrode, its phase led that of the applied voltage by about 90°) and the current spike. The streamer propagation and glow-like discharge caused the current spikes during positive- and negative-going cycles. The intensity of the current spikes during the positive-going cycle was larger than that during negative-going cycle in all cases due to the fact that the bottom-side electrode was buried.

It was also confirmed that the number of current spikes increased with the frequency of the applied voltage. The power dissipated by the microplasma electrode was measured using the charge-voltage curve (Lissajous figure). The Lissajous figure corresponding to an AC voltage with amplitude 1 kV and 1 kHz is shown in **Figure 15**. The measured power consumption was estimated at 0.27 W. At lower frequencies in the 10–100 Hz range, the Lissajous figure could not be obtained, thus power consumption was estimated by multiplying the applied voltage and discharge current.

The power consumption versus the frequency of the applied voltage is shown in **Figure 16**. At 1 kHz the power consumption was calculated to be 0.28 W which was almost the same value calculated using the Lissajous figure.

With the increase of frequency, the power consumption increased. This can be explained by the dielectric barrier discharge phenomena: discharges occurred at the time the polarity of the voltage was inverted, thus discharges per unit time increased.

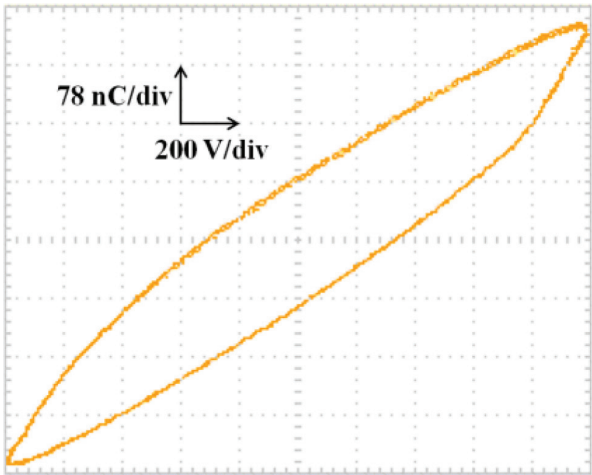


Figure 15.
Lissajous figure when AC voltage with a voltage of 1 kV and a frequency of 1 kHz was applied to the electrode.

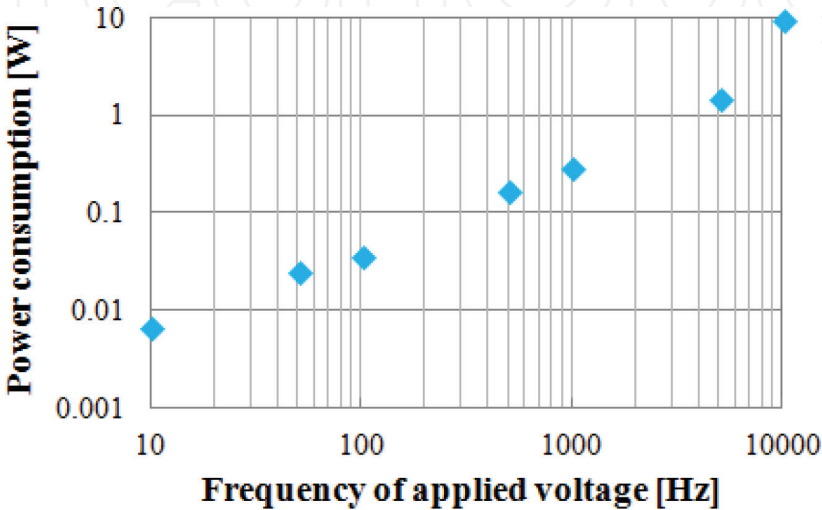


Figure 16.
Power consumption as a function of the frequency of the applied voltage.

2.3.2 Particle removal by microplasma

The SiO₂ particle removal process was investigated when the electrode was energized at an AC voltage with a frequency of 10 Hz, 100 Hz, 1 kHz, and 10 kHz as shown in **Figure 17**. After 5 s, the number of removed particles increased as the frequency increased because more ions were generated at high frequency. With the increase of process time the amount of removed particles decreased as the frequency of the applied voltage increased. Some amount of particles still remained on the electrode surface at high frequency such as 1 and 10 kHz because at high frequency, movement of fine particles could not follow the high-speed inversion of

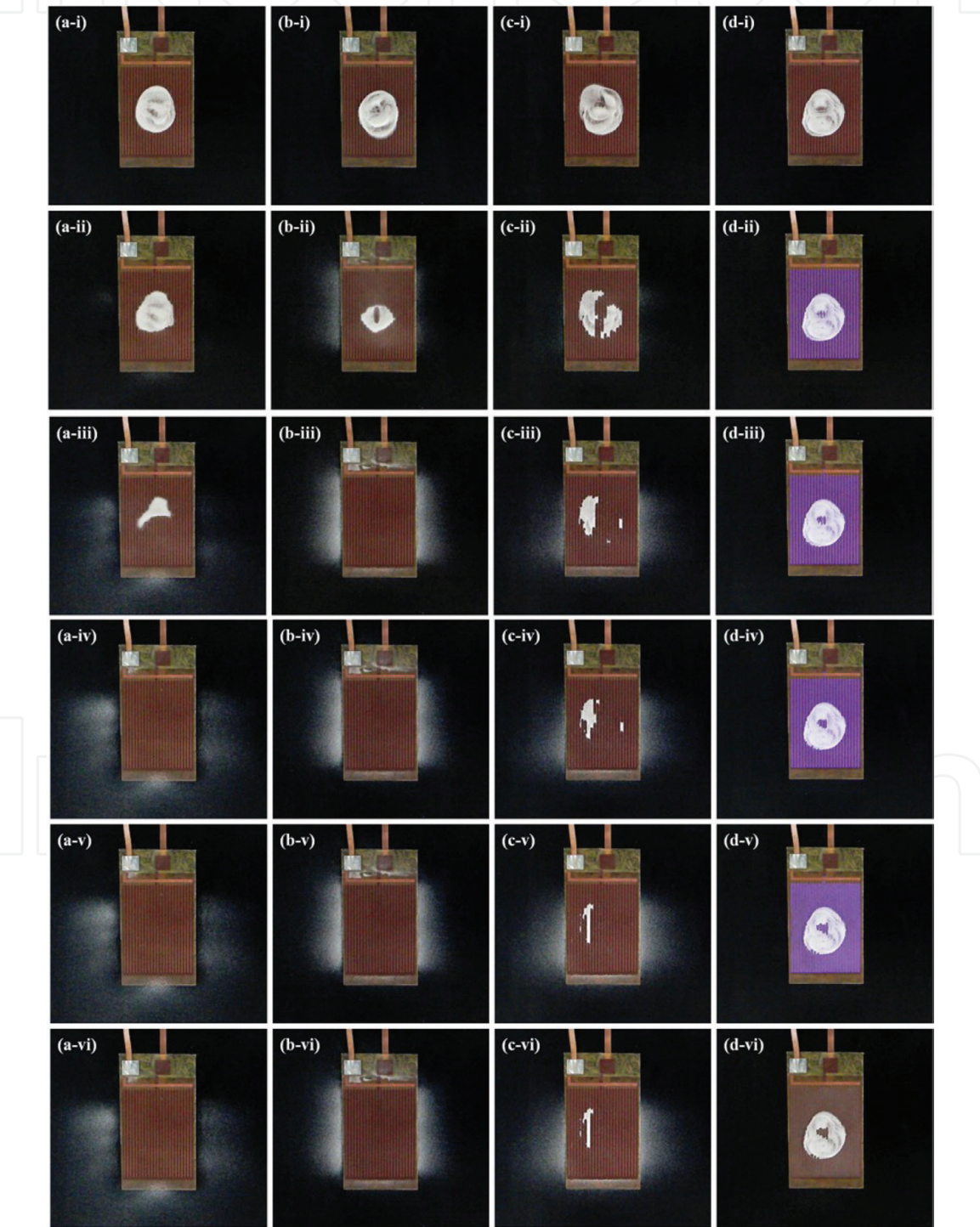


Figure 17. SiO₂ particle movement when the frequencies were set to (a) 10 Hz, (b) 100 Hz, (c) 1 kHz, and (d) 10 kHz: (i) before applying the voltage, after applying voltage for (ii) 1 s, (iii) 5 s, (iv) 10 s, (v) 1 minute, and (vi) 3 minutes.

the polarity. The same phenomena was reported by Kawamoto et al. [19, 20] which carried out fine particle removal and transport and reported that the cleaning efficiency decreased at more than 10 Hz. The threshold value reported in [19, 20] was different from these results obtained at 500 Hz due to the different conditions such as electrode configuration, applied voltage, particle diameter, and electrical properties of particles. The removal rate was defined as

$$\text{Removal rate [\%]} = \frac{(\text{The mass of the particles removed to outside part})}{(\text{The mass of the particles placed on the electrode (60 mg)})} \times 100 \quad (4)$$

The removal rate at various frequencies is shown in **Figure 18**. Each value represents the mean value obtained after three experiments at each frequency. The removal rate for frequencies between 10 and 500 Hz was about 95%, and for frequencies above 500 Hz, the removal rate decreased with the increase of frequency; thus 72% was measured at 1 kHz and 17% at 10 kHz, respectively. Considering also the power consumption, the removal efficiency was high at low frequency.

The process of particle transfer could be described as:

- i. Microplasma was generated at the electrode surface by applying the AC high voltage to the electrode.
- ii. The electrical charging of SiO₂ particles was due to the contact with the electrode and microplasma.
- iii. The Coulomb and dielectrophoretic forces acted on the charged SiO₂ particles.
- iv. With every high-voltage cycle, the processes (ii) and (iii) were repeated, thus SiO₂ particles were transferred to the outside part of the electrode.

After the series of experiments, the following conclusions were obtained:

- 1. The power consumption of the microplasma electrodes increased with the increase of the frequency of the applied voltage.

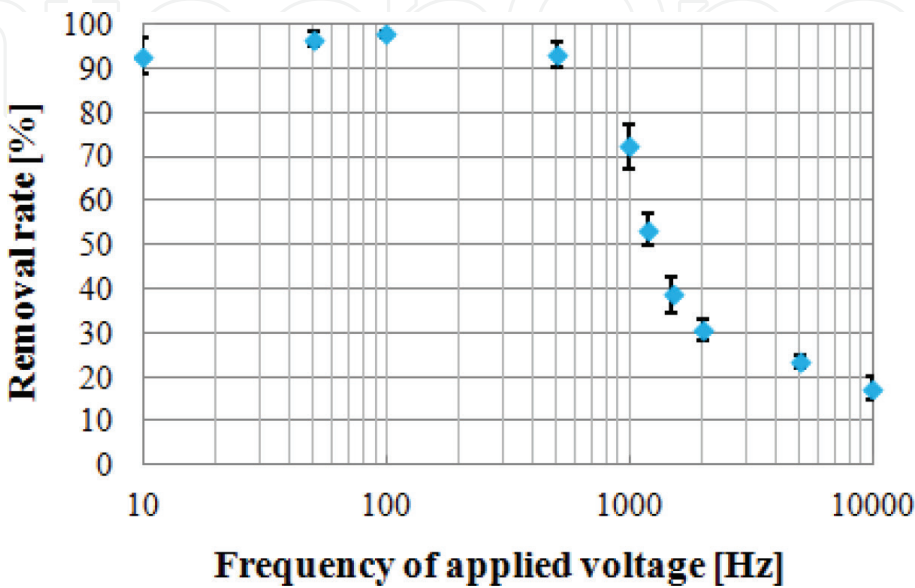


Figure 18.
Removal rate as a function of the frequency of the applied voltage.

2. The removal rate of SiO_2 particles decreased with the increase of frequency. For frequencies between 10 and 500 Hz, the removal rate was about 95%, but the removal rate decreased when the frequency was 500 Hz or above. At 10 kHz 83% particles remained on the electrode surface due to the fact that the SiO_2 particles movement could not follow the polarity changes.

2.4 Microplasma actuator for flow control

Plasma actuators could be a safer and more efficient alternative to conventional mechanical actuators used on aircraft due to their lack of moving parts, simple construction, and fast response due to the electric field [56]. A general classification could split plasma actuators in dielectric barrier discharge (DBD) type and corona discharge type. The induced flow values could reach 7 m/s in the case of single DBD plasma actuator and 11 m/s when a multiple DBD plasma actuator was used [24]. Corona discharge plasma actuators could be used for high-speed flow control where an induced flow speed of more than 7 m/s is required [57–61]. High voltages of about 7 kV peak-to-peak are required for energizing the millimeter-sized discharge gap of DBD plasma actuators applied to turbulent boundary layer control for skin friction drag reduction [62–65]. Research has been done on dielectric barrier discharge (DBD) plasma actuators. This type of plasma actuator is conventionally energized at voltages of tens of kilovolts [22–24]. For flow control applications, a microplasma actuator which can be energized at only 1 kV was developed; thus only a smaller-sized power supply is necessary to energize the actuator, and there are no difficulties of electrically insulating the high voltage.

The induced flow by microplasma actuator occurs due to electrohydrodynamic (EHD) phenomenon through which by collision the momentum is transferred from ions accelerated by the electric field to neutral molecules [22–24].

Microplasma actuator has small dimensions; thus the EHD flow measurements are difficult to carry out. Besides the experimental investigation, numerical simulation software was developed to study the microplasma actuator phenomena especially near the electrode surface where, due to the light emission, the measurements were difficult [25–28].

For the numerical simulation of the flow, the Suzen-Huang model coupled with Navier-Stokes equations was used [66–68]. Other researchers obtained numerical simulation results close to the physical phenomena of the plasma actuator using the Suzen-Huang model [69–71].

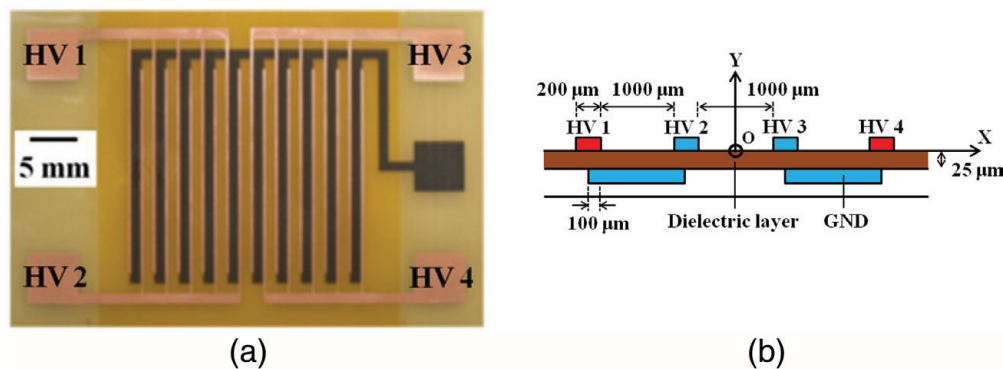


Figure 19. Multi-electrode microplasma actuator. (a) Top view showing strip-like electrodes: HV as energized electrodes and GND as ground; (b) Schematic cross-section view.

2.4.1 Microplasma actuator

The schematic image of microplasma actuator is shown in **Figure 19**. It has a multielectrode structure which allows various parts of the actuator to be energized at different potentials or waveforms, thus obtaining different flow patterns.

The energized top-side electrode has 20 strip-like electrodes with a width of 200 μm and thickness of 16 μm made from copper and placed above a plate type grounded electrode also made from copper. A dielectric layer of resin film with a thickness of 25 μm is placed in between the strip-like electrodes and plate type electrode.

Microplasma actuator is composed of four active parts as shown in **Figure 19**, which can be driven independently. In the series of experiments, an AC voltage with amplitude 1.4 kV and frequency 20 kHz was applied to the parts HV1 and HV4. The applied voltage was pulse-modulated with 50% duty ratio and a burst frequency of 4 kHz. Parts HV1 and HV4 were energized by the AC voltage for 50 ms.

For the flow measurements using the particle tracking velocimetry method (PTV), incense smoke composed from 0.3 μm tracer particles and a laser (Nd YVO₄ 532 nm) were used. The induced flow by the microplasma actuator was measured with a high-speed camera of 1280 \times 128 pixel resolution. The recording frequency of the high-speed camera was at 4000 Hz. The PTV results were obtained using two consecutive images.

2.4.2 Flow control by microplasma actuator

The active electrode parts HV1 and HV4 were energized by a pulse-modulated AC voltage with amplitude 1.4 kV, frequency 20 kHz, and duty ratio 50%.

As shown in **Figure 20**, at time $t = 1$ ms, the vortexes appeared near the strip-like energized electrodes having a counterclockwise direction for the HV1 part and clockwise direction for the HV4 part.

Gradually in time the vortexes above part HV1 and part HV4 unite and form a flow directed toward the right for the HV1 part and toward left above the HV4 part. Furthermore, these two flows collide in the center part of the actuator, and upward flow is formed as shown in **Figure 20** at $t = 10$ ms. The PTV results from **Figure 21**

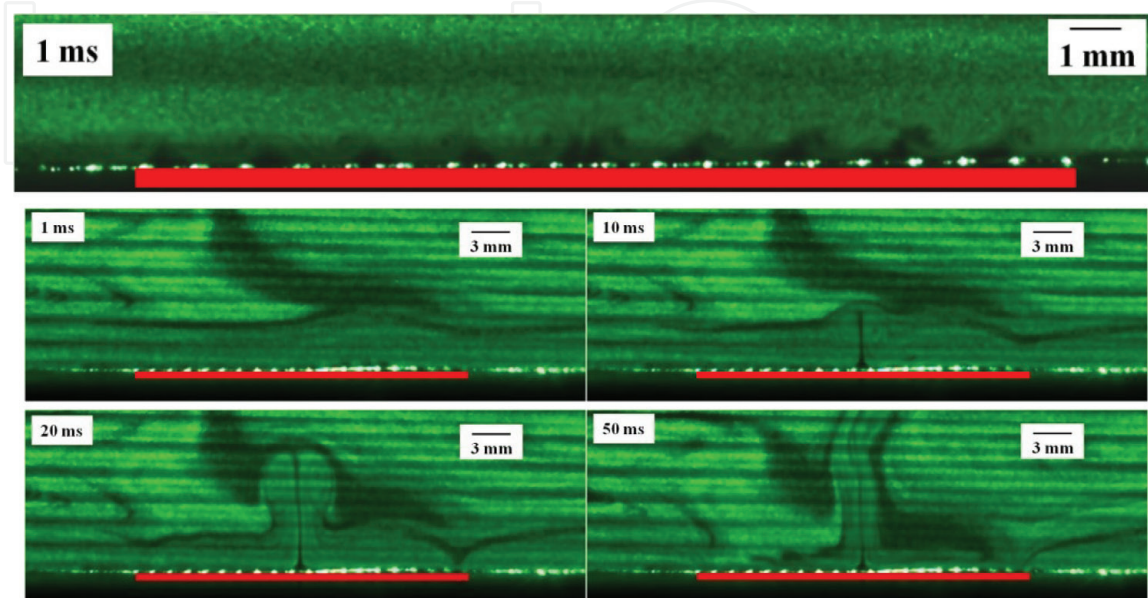


Figure 20.
 Images of generated flow by microplasma actuator. Up to 10 ms vortexes appeared above the active electrodes. After 10 ms upward flow is obtained.

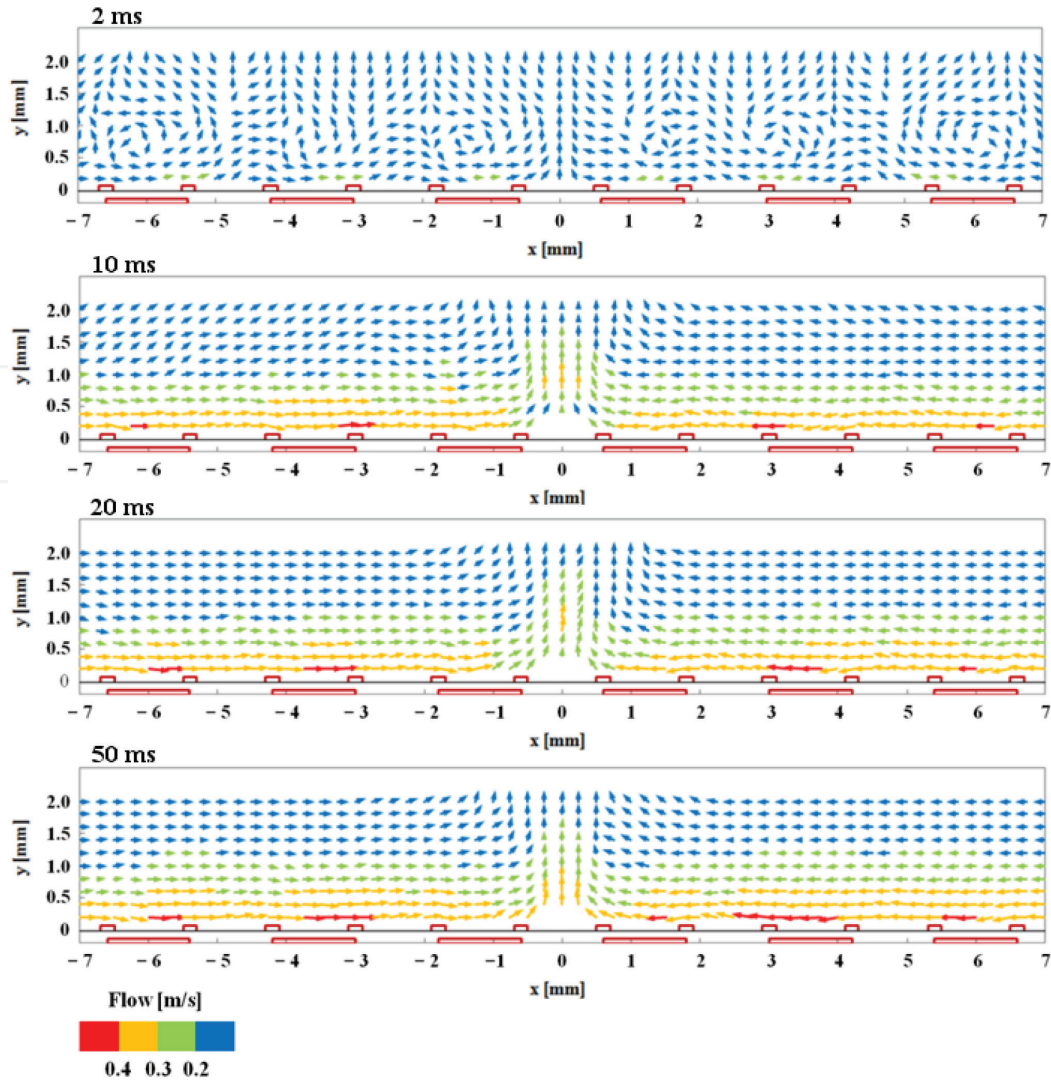


Figure 21.

PTV results of generated flow by microplasma actuator. The maximum flow velocity was measured above the active electrodes.

show the maximum values of flow velocity near the electrodes which at $t = 2$ ms was about 0.3 m/s and at $t = 10$ ms was about 0.5 m/s.

In the center part of the actuator the maximum value was about 0.4 m/s.

Near the active electrodes due to the microplasma light emission, the measurements were difficult to carry out; thus numerical simulations could give additional information about the flow. Numerical simulation code based on the Suzen-Huang model [66–68] was developed. Microplasma is an atmospheric pressure weakly ionized nonthermal plasma; thus the model considers the potential V to be composed from two potentials: the external electric field potential ϕ and the net charge density potential φ . Furthermore the body force was calculated based on these potentials.

Figure 22 shows the geometry used for numerical simulation. For the dielectric the permittivity was $\epsilon_r = 4$ and for the air the permittivity was $\epsilon_{\text{air}} = 1$. Furthermore the harmonic mean of the permittivity was calculated for the conservation of the electric field [67]. The grounded electrodes were considered as source charge, and the value of the source charge was $\rho_c = 0.00752 \text{ C/m}^3$. The value of Debye length was $\lambda_D = 0.00017 \text{ m}$ for the air and $\lambda_D = \infty$ for the dielectric [67]. In order to obtain the flow, the calculated body force F_x and F_y on the x - and y -axes, respectively, were introduced in the Navier-Stokes equations.

The flow velocity has the components u and v on x -axes and y -axes, respectively. The dynamic viscosity μ was calculated with the value of air density $\rho = 1.177 \text{ kg/m}^3$

and the value of kinematic viscosity $\nu = 1.57 \times 10^{-5} \text{ m}^2/\text{s}$; thus dynamic viscosity was $\mu = 1.8 \times 10^{-5} \text{ kg/m s}$.

There was no wall on the left, right, and upper part.

The numerical calculations were carried out for six active electrodes (three for HV1 and three for HV4) with grid dimensions $14 \times 14 \text{ mm}$ and 561×561 grid nodes as shown in **Figure 22**.

The active electrodes were energized by an AC waveform with amplitude 1 kV, 20 kHz, and duty ratio 50%. The body force magnitude and direction according to the “push-push” theory are similar for the positive and negative half-cycles [68]. Because the effective value of AC voltage with 1.4 kV amplitude is 1 kV, we have considered for the numerical simulation a positive pulse signal with peak value of 1 kV with duty ratio 50% as shown in **Figure 23**.

For the equations of potentials and body force which were solved before using the Navier-Stokes equations, the finite difference method was used for the discretization. The calculated body force had the highest intensity near the active electrodes.

Vortexes appeared in the initial stages of discharge near the energized electrodes as shown in **Figure 24**. The vortexes were rotating counterclockwise for the Ch1 electrodes and clockwise for the Ch4 electrodes up to 10 ms. With the lapse of time, after 10 ms the vortexes start to unite on the left side and right side of the microplasma actuator; thus over the Ch1 electrodes, the resultant flow was rightward flow, and leftward flow was obtained on the right side of the actuator over the Ch4 electrodes. The obtained flows collide in the center part of the actuator and an upward flow resulted in that region. The maximum value of the flow was about 0.5 m/s and was calculated near the active electrodes at 1 ms. At 10 ms the maximum value increased to about 0.7 m/s. In the center region the upward flow maximum value was about 0.45 m/s and was obtained after 20 ms. The calculation was carried out up to 50 ms when it can be observed that the upward flow extends up to the upper part of the calculation geometry boundary. At up to 0.2 mm height from the active electrodes, the microplasma light emission influenced the measurement; thus the experimental data in that region was not accurate. The numerical results gave us additional information about the flow near the active electrodes region.

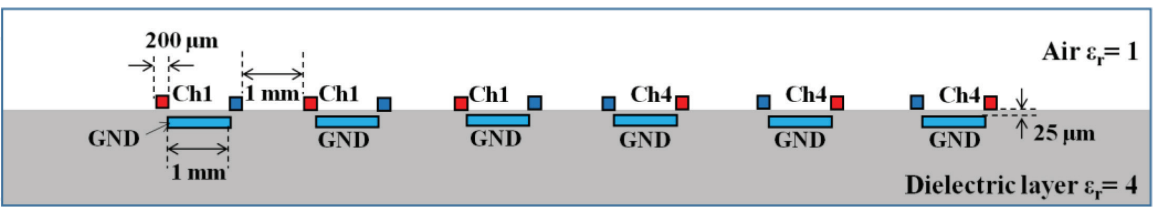


Figure 22.
Computational geometry. Ch1 and Ch4 electrodes were energized.

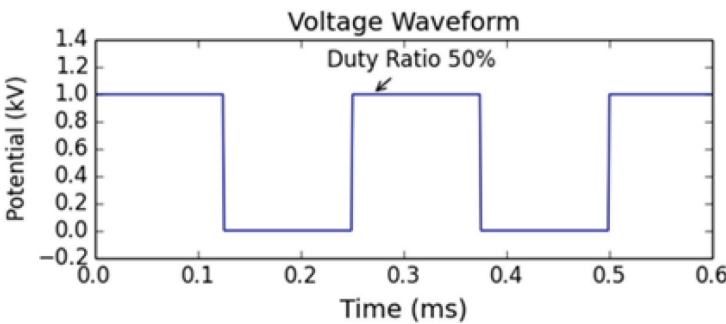


Figure 23.
Voltage waveform.

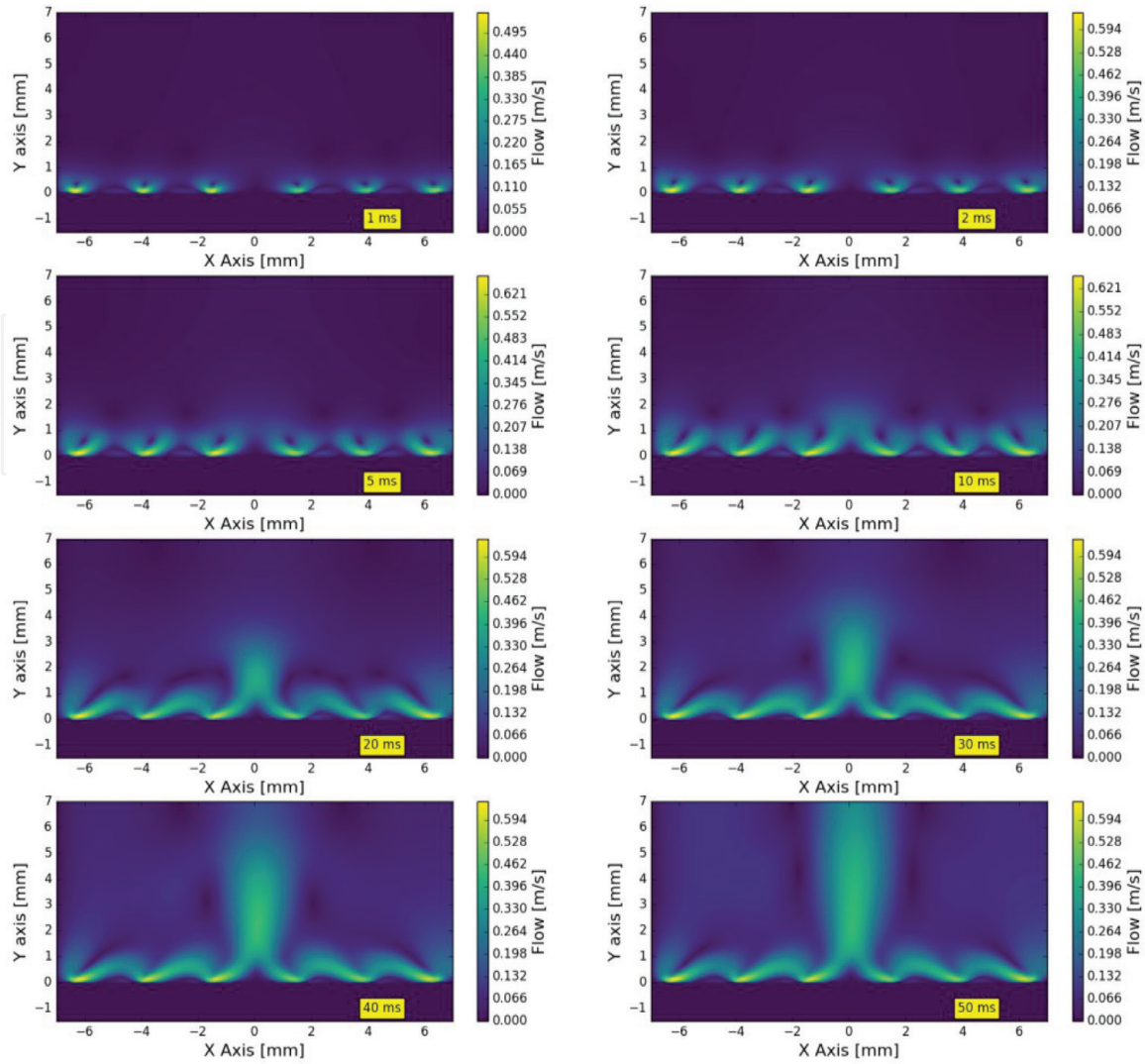


Figure 24.
Induced flow by the microplasma actuator.

The comparison between the experimental results and numerical simulation results shows a good fit considering the flow characteristics and values. The numerical simulation data was more accurate than the experimental results near the active electrodes region.

The duty ratio was 50% for the HV1 and HV4 electrodes, thus the obtained flow was an upward flow. By changing the duty ratio of electrodes or energizing other parts (HV2 or HV3), the flow direction can be changed.

3. Conclusions

Dielectric barrier discharge microplasma has proven to be a technology with various applications that can replace classical technologies for indoor air purification, drug delivery, particles removal and induced flow. Microplasma can be generated at voltages of about 1 kV making this technology safer, cheaper and easier to insulate and integrate in other systems compared with classical non-thermal plasma technologies which requires tens of kilovolts. The low discharge voltage requires a smaller-sized power supplies which also contributes to the miniaturization of the system. The electrodes can be scaled up to large areas depending on the applications requirements without increasing the discharge voltage and in the case of microplasma actuator the flexible-type electrode can be bent in various shapes to the surface.

The microplasma process of hexadecane removal decreased the concentration of hexadecane from the initial value of 3000 ppm to 150 ppm after the 120 minutes of microplasma treatment. In comparison, the natural decay was decreasing to 950 ppm.

The plasma treatment of pig skin decreased to one-third (11 μm) that of the original thickness after 60 s of treatment. After 30 s of treatment, the skin was disrupted, and the saturation of etching effect was observed after 120 s.

The removal of SiO_2 particles from the surface of microplasma electrode decreased with the increase of frequency. For frequencies between 10 and 500 Hz, the removal rate was about 95%, but the removal rate decreased when the frequency was 500 Hz or above.

The microplasma actuator induced an upward flow, while the electrode was energized with a duty ratio of 50% in both left part and right part of the actuator. The simulation results were confirmed by experimental results.

Acknowledgements


The authors would like to thank Professor Hitoki Yoneda from the University of Electro-Communications, Tokyo, Professor Damon Chandler, Mr. Yoshinori Mizuno, Mr. Akihiko Ito, and Mr. Daisuke Nonaka from Shizuoka University, Hamamatsu, for the fruitful discussions.

Author details

Kazuo Shimizu*, Jaroslav Kristof and Marius Gabriel Blajan
Shizuoka University, Hamamatsu, Japan

*Address all correspondence to: shimizu@cjr.shizuoka.ac.jp

IntechOpen

© 2018 The Author(s). Licensee IntechOpen. This chapter is distributed under the terms of the Creative Commons Attribution License (<http://creativecommons.org/licenses/by/3.0>), which permits unrestricted use, distribution, and reproduction in any medium, provided the original work is properly cited. 

References

- [1] Iza F, Kim GJ, Lee SM, Lee JK, Walsh JL, Zhang YT, et al. Microplasmas: Sources, particle kinetics, and biomedical applications. *Plasma Processes and Polymers*. 2008;**5**(4):322-344
- [2] Foest R, Schmidt M, Becker K. Microplasmas: An emerging field of low-temperature plasma science and technology. *International Journal of Mass Spectrometry*. 2006;**248**(3):87-102
- [3] Shimizu K, Ishii T, Blajan M. Emission spectroscopy of pulsed power microplasma for atmospheric pollution control. *IEEE Transactions on Industry Applications*. 2010;**46**(3):1125-1131
- [4] Blajan M, Umeda A, Muramatsu S, Shimizu K. Emission spectroscopy of pulsed powered microplasma for surface treatment of PEN film. *IEEE Transactions on Industry Applications*. 2011;**47**(3):1100-1107
- [5] Orosa J. Indoor and Outdoor Air Pollution. Rijeka, Croatia: InTech; 2011
- [6] Arashidani K, Akiyama Y, Kunugita N. Study of indoor air pollution. *Indoor Environment*. 2009;**12**(2):71-86
- [7] Weschler CJ. Changes in indoor pollutants since the 1950s. *Atmospheric Environment*. 2009;**43**:153-169
- [8] Eliasson B, Hirth M, Kogelschatz U. Ozone synthesis from oxygen in dielectric barrier discharges. *Journal of Physics D: Applied Physics*. 1987;**20**(11):1421-1437
- [9] Lerouge S, Fozza AC, Wertheimer MR, Marchand R, Yahia LH. Sterilization by low-pressure plasma: The role of vacuum-ultraviolet radiation. *Plasmas and Polymers*. 2000;**5**(1):31-46
- [10] Moisan M, Barbeau J, Moreau S, Pelletier J, Tabrizian M, Yahia L'H. Low-temperature sterilization using gas plasmas: A review of the experiments and an analysis of the inactivation mechanisms. *International Journal of Pharmaceutics*. 2001;**226**:1-21
- [11] Shimizu K. Indoor air control by microplasma. In: Farhad Nejadkoorki, editor. *Advanced Air Pollution*. IntechOpen; 2011. pp. 509-535. DOI: 10.5772/16764. Available from: <https://www.intechopen.com/books/advanced-air-pollution/indoor-air-control-by-microplasma>
- [12] Lademann J, Patzelt A, Richter H, Lademann O, Baier G, Breucker L, et al. Nanocapsules for drug delivery through the skin barrier by tissue-tolerable plasma. *Laser Physics Letters*. 2013;**10**:083001
- [13] Shimizu K, Hayashida K, Blajan M. Novel method to improve transdermal drug delivery by atmospheric microplasma irradiation. *Biointerphases*. 2015;**10**:029517
- [14] Kalghatgi S, Tsai C, Gray R, Pappas D. Transdermal drug delivery using cold plasmas. In: 22nd International Symposium on Plasma Chemistry. July 5-10, 2015
- [15] Kristof J, An NT, Miyamoto H, Blajan MG, Shimizu K. Skin permeability and transdermal drug delivery by plasma irradiation. In: Proc. 18th Takayanagi Kenjiro Memorial Symposium. Hamamatsu, Japan: Shizuoka Univ.; Nov. 15-16, 2016
- [16] Hattori T. Contamination control: Problems and prospects. *Solid State Technology*. 1990;**33**(7):S1-S8
- [17] Christoffersen R, Lindsay JF, Noble SK, Meador MA, Kosmo JJ, Lawrence JA, et al. NASA=TP-2009-214786; 2009

- [18] Calle CI, McFall JL, Buhler CR, Snyder SJ, Arens EE, Chen A, et al. Proc. ESA Annu. Meet. Electrostatics; 2008
- [19] Kawamoto H, Miwa T. Mitigation of lunar dust adhered to mechanical parts of equipment used for lunar exploration. *Journal of Electrostatics*. 2011;**69**:365
- [20] Mazumder M, Horenstein M, Stark J, Hudelson JN, Sayyah A, Heiling C, et al. Proc. IAS Annu. Meet., 2014. 2014-EPC-0305
- [21] Kawamoto H, Shibata T. Electrostatic cleaning system for removal of sand from solar panels. *Journal of Electrostatics*. 2015;**73**:65
- [22] Roth JR, Sherman DM, Wilkinson SP. Boundary Layer Flow Control with a One Atmosphere Uniform Glow Discharge Surface Plasma. AIAA 98-0328. 1998
- [23] Roth JR, Din X. Optimization of the aerodynamic plasma actuator as an electrohydro-dynamic (EHD) electrical device. AIAA, 44th AIAA Aerospace Sciences Meeting and Exhibit, 9-12 Jan., 2006
- [24] Benard N, Moreau E. Electrical and mechanical characteristics of surface AC dielectric barrier discharge plasma actuators applied to airflow control. *Experiments in Fluids*. 2014;**55**:1846. DOI: 10.1007/s00348-014-1846-x
- [25] Shimizu K, Mizuno Y, Blajan M, Yoneda H. Characteristics of an atmospheric nonthermal microplasma actuator. *IEEE Transactions on Industry Applications*. 2017;**53**(2):1452-1458
- [26] Blajan M, Mizuno Y, Ito A, Shimizu K. Microplasma actuator for EHD induced flow. *IEEE Transactions on Industry Applications*. 2017;**53**(3):2409-2415
- [27] Blajan M, Ito A, Kristof J, Shimizu K. Flow control by dielectric barrier discharge microplasma. In: Luca D, Sirghi L, Costin C, editors. *Recent Advances in Technology Research and Education. INTER-ACADEMIA 2017. Advances in Intelligent Systems and Computing*. Vol. 660. Cham: Springer; 2018
- [28] Nguyen HP, Park MJ, Kim SB, Kim HJ, Baik LJ, Jo YM. Effective dielectric barrier discharge reactor operation for decomposition of volatile organic compounds. *Journal of Cleaner Production*. 2018;**198**:1232-1238
- [29] Holzer F, Kopinke F-D, Roland U. Non-thermal plasma treatment for the elimination of odorous compounds from exhaust air from cooking processes. *Chemical Engineering Journal*. 2018;**334**:1988-1995
- [30] Van Durme J, Dewulf J, Sysmans W, Leys C, Van Langenhove H. Abatement and degradation pathways of toluene in indoor air by positive corona discharge. *Chemosphere*. 2007;**68**:1821-1829
- [31] Jung J-S, Kim J-G. An indoor air purification technology using a non-thermal plasma reactor with multiple-wire-to-wire type electrodes and a fiber air filter. *Journal of Electrostatics*. 2017;**86**:12-17
- [32] Shimizu K, Muramatsu S, Kristof J, Blajan M. Analysis of hexadecane decomposition by atmospheric microplasma. *IEEE Transactions on Industry Applications*. 2018;**54**(1):605-610
- [33] Shimizu K, Kuwabara T, Blajan M. Study on decomposition of indoor air contaminants by pulsed atmospheric microplasma. *Sensors*. 2012;**12**:14525-14536
- [34] Shimizu K, Kurokawa Y, Blajan M. Study of VOC removal and *E. coli* sterilization in six-mat space by atmospheric microplasma. In: Proc. Int.

Conf. IEEE Ind. Appl. Soc., 2015-EPC-0512, Addison, TX, USA. 2015

[35] Nejadkoorki F. Advanced Air Pollution. Rijeka, Croatia: InTech; 2011. p. 584

[36] Shimizu K, Blajan M, Tatematsu S. Basic study of remote disinfection and sterilization effect by using atmospheric microplasma. IEEE Transactions on Industry Applications. 2012;**48**(4):1182-1188

[37] Blajan M, Shimizu K. Temporal evolution of dielectric barrier discharge microplasma. Applied Physics Letters. 2012;**101**:104101

[38] Aleknaviciute I. Plasma assisted decomposition of methane and propane and cracking of liquid hexadecane [Ph.D. dissertation]. Uxbridge, U.K.: School Eng. Design, Brunel Univ.; 2013. [Online]. Available from: <http://bura.brunel.ac.uk/handle/2438/8574>

[39] Kristof J, Miyamoto H, Tran AN, Blajan M, Shimizu K. Feasibility of transdermal delivery of cyclosporine a using plasma discharges. Biointerphases. 2017;**12**(2):02B402-1-02B402-11

[40] Shimizu K, Tran AN, Blajan M. Effect of microplasma irradiation on skin barrier function. Japanese Journal of Applied Physics. 2016;**55**(1):07LG01

[41] Kalghatgi S, Tsai C, Gray R, Pappas D. 22nd International Symposium on Plasma Chemistry. Antwerp, Belgium; 5-10 July 2015. p. O-22-6

[42] Szili EJ, Bradley JW, Short RD. A 'tissue model' to study the plasma delivery of reactive oxygen species. Journal of Physics D: Applied Physics. 2014;**47**:152002

[43] Kartaschew K, Mischo M, Baldus S, Brundermann E, Awakowicz P, Havenith M. Unraveling the interactions

between cold atmospheric plasma and skin-components with vibrational microspectroscopy. Biointerphases. 2015;**10**:029516

[44] Marschewski M, Hirschberg J, Omairi T, Viol W, Emmert S, Maus-Friedrichs W. Electron spectroscopic analysis of the human lipid skin barrier: Cold plasma-induced changes in lipid composition. Experimental Dermatology. 2012;**21**:921

[45] Rai V, Ghosh I, Bose S, Silva SMC, Chandra P, Michniak-Kohn B. A transdermal review on permeation of drug formulations, modifier compounds and delivery methods. Journal of Drug Delivery Science and Technology. 2010;**20**:75-87

[46] Hill JR, Wertz PW. Molecular models of the intercellular lipid lamellae from epidermal stratum corneum. Biochimica et Biophysica Acta. 2003;**1616**:121. DOI: 10.1016/S0005-2736(03)00238-4

[47] Tachibana K. IEEJ Transactions on Electrical and Electronic Engineering. 2006;**1**:145

[48] Lauer JL, Shohet JL, Albrecht RM, Pratoomtong C, Murugesan R, Esnault S, et al. Journal of Applied Physics. 2004;**96**:4539

[49] Szili EJ, Al-Bataineh SA, Bryant PM, Short RD, Bradley JW, Steele DA. Plasma Processes and Polymers. 2011;**8**:38

[50] Mariotti D, Sankaran RM. Journal of Physics D. 2010;**43**:323001

[51] Melcher JR, Warren EP, Kotal RH. IEEE Transactions on Industry Applications. 1989;**25**:956

[52] Kawamoto H, Hasegawa N. Journal of Imaging Science and Technology. 2004;**48**:404

- [53] Kern W. Journal of the Electrochemical Society. 1990;**137**:1887
- [54] Zhang F, Busnaina AA, Fury MA, Wang S-Q. Journal of Electronic Materials. 2000;**29**:199
- [55] Shimizu K, Ito A, Blajan M, Kristof J, Yoneda H. Basic study of fine particle removal using microplasma and its electrostatic effect. Japanese Journal of Applied Physics. 2017;**56**:01AC03. DOI: 10.7567/JJAP.56.01AC03
- [56] Blajan M, Ito A, Kristof J, Shimizu K. Directional flow control with multielectrode system microplasma actuator. Journal of Biomedical Systems and Emerging Technologies. 2017;**4**:116
- [57] Zhao L, Adamiak K. Electrohydrodynamic flow produced by electric corona discharge (numerical and experimental studies, and applications). In: Proc. 2009 Electrostatics Joint Conference. Vol. 13. Boston, America, P2; 2010. pp. 16-18
- [58] Colas DF, Ferret A, Pai DZ, Lacoste DA, Laux CO. Ionic wind generation by a wire-cylinder-plate corona discharge in air at atmospheric pressure. Journal of Applied Physics. 2010;**108**:103306
- [59] Robinson M. Movement of air in the electric wind of the corona discharge. Transactions of the American Institute of Electrical Engineers. 1961;**80**:143-150
- [60] June MS, Kribs J, Lyons KM. Measuring efficiency of positive and negative ionic wind devices for comparison to fans and blowers. Journal of Electrostatics. 2011;**69**:345-350
- [61] Kim C, Park D, Noh KC, Hwang J. Velocity and energy conversion efficiency characteristics of ionic wind generator in a multistage configuration. Journal of Electrostatics. 2010;**68**:36-41
- [62] Touchard G. Plasma actuators for aeronautics applications—State of art review. International Journal of Plasma Environmental Science & Technology. 2008;**2**:1-25
- [63] Whalley RD, Choi KS. The starting vortex in quiescent air induced by dielectric-barrier-discharge plasma. Journal of Fluid Mechanics. 2012;**703**:192-203
- [64] Whalley RD, Choi KS. Turbulent boundary-layer control with plasma spanwise travelling waves. Experiments in Fluids. 2014;**55**:1796
- [65] Choi KS, Jukes T, Whalley R. Turbulent boundary-layer control with plasma actuators. Philosophical Transactions of the Royal Society A. 2011;**369**:1443-1458
- [66] Suzen YB, Huang PG, Jacob JD, Ashpis DE. Numerical simulations of plasma based flow control applications. In: 35th Fluid Dynamics Conference and Exhibit. Toronto, Ontario; June 6-9, 2005. AIAA 2005-4633
- [67] Suzen YB, Huang PG, Ashpis DE. Numerical simulations of flow separation control in low-pressure turbines using plasma actuators. In: 45th AIAA Aerospace Sciences Meeting and Exhibit. Reno, Nevada; 8-11 January 2007. AIAA 2007-937
- [68] Orlov DM. Modelling and Simulation of Single Dielectric Barrier Discharge Plasma Actuator [PhD Thesis]. University of Notre Dame; 2006
- [69] Maden I, Maduta R, Kriegseis J, Jakirlic S, Schwarz C, Grundmann S, et al. Experimental and computational study of the flow induced by a plasma

actuator. *International Journal of Heat and Fluid Flow*. 2013;**41**:80-89

[70] Abdollahzadeh M, Pascoa JC, Oliveira PJ. Modified split-potential model for modeling the effect of DBD plasma actuators in high altitude flow control. *Current Applied Physics*. 2014;**14**:1160-1170

[71] Brauner T, Laizet S, Benard N, Moreau E. Modelling of dielectric barrier discharge plasma actuators for direct numerical simulations. In: *AIAA Aviation*. Washington, D.C.: 8th AIAA Flow Control Conference; 13-17 June 2016. AIAA 2016-3774